Nanotechnology for Environmental Engineering (2020) 5:14
https://doi.org/10.1007/s41204-020-00078-w

ORIGINAL PAPER

Synthesis of copper oxide nanoparticles by chemical and biogenic methods: photocatalytic degradation and in vitro antioxidant activity

A. Muthuvel[1] · M. Jothibas[1] · C. Manoharan[2]

Received: 26 March 2020 / Accepted: 30 May 2020 / Published online: 7 June 2020

Abstract
Copper oxide nanoparticles (CuO-NPs) were synthesized using two different methods (chemical and biosynthesis) to study the influence of the preparation method on the structural, optical, morphological, photocatalyst, antibacterial and in vitro antioxidant of these nanoparticles. The synthesized nanoparticles were analysed by XRD, UV–Vis, HR-TEM, DLS, ZE, PL and FT-IR spectroscopy. The X-ray diffraction spectra showed the single-phase monoclinic structure of copper oxide, with an average crystallite size of 2.05–3.00 nm. HR-TEM analysis confirmed the spherical morphology of the synthesized CuO-NPs using chemical and biological methods with an average size of 32 nm and 25 nm, respectively. The synthesized CuO-NPs exhibited potential photocatalytic activity towards the degradation of methylene blue dye on exposing to sunlight irradiation. The degradation effectiveness against methylene blue dye was found to be 85 and 97% for chemical and biosynthesized CuO-NPs, respectively. Furthermore, antibacterial and antioxidant activities were evaluated. The biogenic method showed a significant antibacterial activity against Gram-negative bacteria *E. coli* and *B. subtilis* than Gram-positive bacteria and also DPPH assay.

Keywords CuO-NPs · Biosynthesis · *Solanum nigrum* · Photocatalytic · Antibacterial

Introduction

Nanoparticles that are having size less than 100 nm are being extensively utilized in the nanoscience application [1]. Metal and metal oxide nanoparticles are emerging as potential candidate in the field of nanoscience and nanotechnology. Metallic nanoparticles with physical, chemical, electrical and optical properties play a crucial role depending on their size and shape. They find a wide range of application, namely sensors, catalysis, antibacterial, antioxidants, etc. Metal oxide nanoparticles such as, ZnO, CoO, TiO_2, SnO_2 and CuO, have been investigated for their environmental and biomedical application [2]. Especially, copper oxide nanoparticle (CuO-NPs) exhibits high potentiality in the metal oxide nanoparticles due to its low cost, optical, catalytic and antimicrobial properties. CuO-based nanoparticles are regarded as photocatalysts due to their bandgap (1.35–3.5 eV), low toxicity, easy availability, and surface synthesis among various semiconductor photocatalysts under sunlight irradiation [3]. CuO-NPs attracts attention because of its large surface area, enhanced oxygen adsorption capability, high surface and considered as promising candidate with enhanced photocatalytic activity [4]. In CuO-NPs, due to the strong tendency to absorb molecular oxygen, the electron–hole pair rearrangement can be controlled at the interface and plays an important role in the removal of the photogenerated electron [5].

Aquatic toxicity, phototoxicity and metal bioavailability of synthetic dyes pose a serious threat to human health, living resources and ecosystems [6]. One of the most common dye materials used in wood, silk and cotton is methylene blue (MB). The same dye is also used in veterinary medicine and diagnostic as well as therapeutic purpose in the case of human being [7–9]. MB cause eye burns and sometime permanent injury to the eyes. The inhaling of MB leads to difficulty in breathing and sweating, burning sensation in mouth, rapid increase heart rate, excessive sweating, vomiting and headache [10–12]. Therefore, attention should be paid in treating MB with waste products. Though there

✉ M. Jothibas
jothibas1980@gmail.com

[1] PG & Research Department of Physics, T.B.M.L. College, Porayar, Mayiladuthurai, Tamil Nadu 609307, India

[2] Department of Physics, Annamalai University, Annamalai nagar, Cuddalore, Tamil Nadu 608002, India

are many conventional methods available for the removal of dye from industrial wastewater, they are not completely efficient because they convert pollutant from one form to another [13]. Sunlight source photocatalytic reaction of organic hazardous compounds is better for water treatment approach. Various methods like physical, chemical, biological and hybrid method are used to synthesise CuO-NPs. The popular methods to the synthesis of CuO-NPs are physical and chemical methods. These are extremely costly methods and use toxic and hazardous chemicals. They are not environmental friendly. The sol–gel technique [14], chemical reduction technique [15], co-precipitation [16], microwave-assisted heating routes [17] and radiolytic process [18] are developed to the synthesis of CuO-NPs chemically. Sol–gel technique is preferred, since it involves the reduction of copper nitrate in aqueous solution. It is an effective reducing agent in the presence of appropriate stabiliser, which is necessary in shielding the growth of CuO-NPs through aggregation. It is the best and most easy technique to yield nanoparticles without aggregation, high yield and less expensive [19]. In clinical field, the use of toxic chemical limits the biomedical application. In addition, when extremely small particles are necessary, the complexity and the cost of manufacturing increase greatly. Hence, the preparation technique is shifted towards 'green' chemistry and bioprocess approach. Nowadays, green package reduces/eliminates the use and production of substance that is hazardous to its nontoxic, cost effective, environmental human health and acts as a bio-compatible reducing agent in the synthesis of CuO-NPs. Recently investigated the synthesis of CuO-NPs using various biological systems such as, honey, egg white, bacteria, fungal and plants extracellular compounds [19]. Among them, the use of extracts from plant materials has attracted the interest of the scientific community, due to their bioactive components, which act as a covering and reducing agent and help to fabricate nanocrystalline metal oxide nanoparticles of different morphologies and size. Earlier reports of green-synthesized CuO-NPs are investigated using plant extract such as *Albizia lebbeck* [20], *Euphorbia esula* [21], *Bifurcaria bifurcate* [22] and *Nerium oleander* [23], *Aspergillus fumigates* [24], *Madhuca longifolia* [25] and *Lemongrass* [26]. Arunkumar et al. [3] have reported that the *Lanatana camara* leaf extract-mediated synthesized CuO-NPs degraded the MB dye at 94% on irradiation with sunlight. Sathiyavimal et al. [27] have reported that the *Sida acuta* leaf extract-mediated synthesized CuO-NPs degraded 93% MB dye in bout 100 min. The biosynthesized CuO-NPs using *Gloriosa superba* leaf extract were examined under Gram-negative and Gram-positive bacteria and relatively more susceptible to the CuO-NPs then *E. coli* bacteria [28]. *Solanum nigrum* is a species in the family Solanaceae. In India, the traditional medicine system uses *Solanum nigrum* in herbaceous perennial plant for its anti-inflammatory, anti-ulcerogenic, anti-tumorigenic and antioxidant characteristics and it could withstand high metal concentration in contaminated soils. It is in great demand in the pharmaceutical industry, since it has tolerance to an adverse environment, and these plants belong to the family of hyperaccumulators, which can attach to heavy metals and play an important role in the reduction mechanism [2]. Synthesis of silver [29] and gold [30] nanoparticles using *Solanum nigrum* leaf extract was reported in literature and, there are no reports available on biosynthesis of CuO-NPs using leaf extracts of *Solanum nigrum.* In the present work, chemically synthesis (Chem) CuO-NPs is compared to the biological method using *Solanum nigrum* leaf extract at various concentrations (5, 10, 15 and 20 ml). The synthesized CuO-NPs are characterized using UV–Vis, XRD, DLS, ZP, HR-TEM and FT-IR spectroscopy. The efficiency of synthesized CuO-NPs photocatalyst for the degradation of MB dye, antibacterial and antioxidant activity by DPPH assay is studied. Here, for the first time, *Solanum nigrum* leaf extract used to biosynthesized CuO-NPs for the MB dye degradation under sunlight irradiation and biomedical application.

Materials and methods

Materials

Leaves of *Solanum nigrum* were collected freshly from rural area of Porayar, Tamil Nadu, India. Copper nitrate ($Cu(NO)_3$), sodium hydroxide (NaOH) and methylene blue ($C_6H_{18}CIN_3S{\bullet}3H_2O$) (Sigma-Aldrich Chemicals, Bangalore, India). Pathogenic bacterial strains were from Institute Microbial Technology, Chandigarh, India. They were maintained in nutrient agar medium (Hi-Media, Mumbai, India). They were reagents used in antimicrobial assay. They had analytical grade with the highest purity and deionized water was used as solvents.

Preparation of leaf extract

Healthy leaves of *Solanum nigrum* were washed several times with deionised water to remove the dust particles on their surface. Initially, 10 g of leaf was slashed to smaller size and stirred with 100 ml of deionized water on heating mantle for 80 °C for 25 min until the colour was changed from watery to brown. The leaf extract was cooled to room temperature and filtered using Whatman filter No: 1 paper and it was collected in 150 ml conical flask and used for further usage.

Chemically synthesis of CuO-NPs

CuO-NPs were prepared by sol–gel method [14]. In a distinctive synthesis, 0.1 M of copper nitrate was prepared in 100 ml of deionized water and stirred constantly until a homogeneous blue colour solution was obtained. 0.2 M NaOH was then added in the solution and stirred ultrasonically for 80 °C for 2 h until a black precipitate was obtained and it was further cooled at room temperature. A great amount of black precipitate was obtained. After precipitation, the precipitate was filtered and washed with the excess methanol to remove starting material. Finally, powder was dried in hot air oven at 400 °C for 4 h, for further characterization.

Biosynthesis of CuO-NPs

Biosynthesis CuO-NPs was prepared by sol–gel method [3]. The 0.1 M copper nitrate was dissolved in deionized water (100 ml) with constant stirring at room temperature. The various concentrations (5, 10, 15 and 20 ml) of aqueous leaf extract solution were added to the copper nitrate solution with continuous stirring at a temperature of 85 °C for 2 h to get colloids. The formation of nanoparticles was revealed by a visual colour of blue to dark black on continuous stirring and black precipitate was obtained. Further, the precipitate was dried at 400 °C for 4 h and the obtained powder was subjected for further characterization. Figure 1 shows the schematic representation of Chem and biosynthesized CuO-NPs.

Characterization of CuO-NPs

CuO-NPs samples were subjected to UV–visible spectroscopy (Shimadu UV-1650) to study the optical respond and to calculate the bandgap. The structural behaviour was determined from X-ray diffraction pattern using Cu Kα radiation ($\lambda = 1.54060$ Å) with nickel monochromatic in the 2θ range

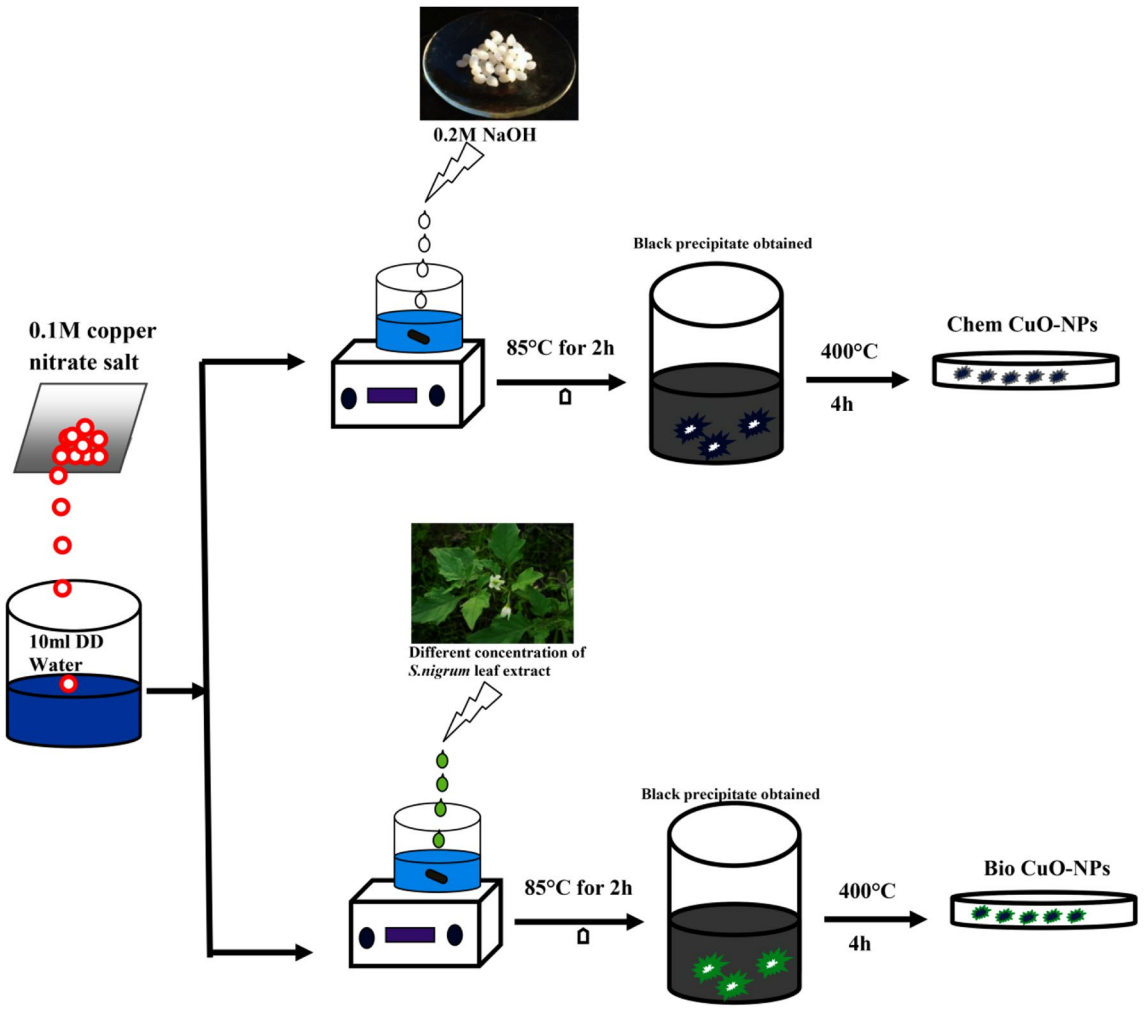

Fig. 1 Schematic representation of chemical and biosynthesized CuO-NPs

started from 20° to 80°. The surface charges (zeta potential) were analyzed and the size distribution and average particle size were observed using the dynamic light scattering (DLS) technique using (Malvern Mansettings Nano). The high-transmission electron microscopy (HR-TEM-PHILLIPS TECNAI G2 FEI 12) was carried out to analysis the particle size, inter planer spacing and shape. The fluorescence analysis was carried out using a Elico S1 174 spectrofluorometer in the range of 200–800 nm. The FT-IR spectra were recorded with an FT-IR (2000) Perkin Elmer using KBr plate at room temperature in the range 4000–400 cm^{-1} with a scanning rate of 4 cm^{-1}/min to identify the presence of functional groups.

Photocatalytic activity

From MB degradation reactions with stimulated sunlight irradiation condition, the photocatalytic activity of Chem CuO-NPs and biosynthesized CuO-NPs was analyzed. In this experiment, 100 ml of 5×10^{-3} M aqueous MB solution and 0.2 g of fine powder catalyst [from Chem CuO-NPs and biosynthesized (10 ml) CuO-NPs] were taken. The measurement period of photocatalytic activity was ranging from 0 to 50 min. To achieve the adsorption, the adsorption–desorption equilibrium in between nanoparticles and dye, the suspension was allowed for stirring in dark for 10 min. Subsequently, the suspension was placed under sunlight radiation and took the reading after every 10 min until 50 min and the colour of the suspension shifted from the blue to colourless. The residual solution was analyzed using UV spectrophotometer. The MB absorbed (%) on the catalyst surface was calculated by from the following [31]:

$$\text{Degradation } (\%) = \frac{C_0 - C_t}{C_0} \times 100\%, \tag{1}$$

where C_0 represents the initial in absorption and C_t represents the absorption after various time intervals (min).

Antibacterial analysis

The antibacterial properties of aqueous leaf extract of *Solanum nigrum*, Chem CuO-NPs and biosynthesized (10 ml) CuO-NPs was investigated using Kirby–Bauer disc diffusion method [30]. This technique utilized a clinically isolated bacterial culture, such as Gram positive (*Bacillus subtilis*, *Staphylococcus saprohyticus*) and Gram negative (*Escherichia coli*, *Pseudomonas aeruginosa*). Bacterial suspension poured into molten nutrient agar sterile cotton cloth poured into stacks sterile wells made with a sterilized stell sterile cork borer. The *Solanum nigrum* leaf extract, Chem CuO-NPs and biosynthesized CuO-NPs were added to the well aseptic conditions at various concentrations (50 and 100 µl). The 25 µg of ciprofloxacin was used as positive control. The plates containing the disks were incubated at 35 °C for 24 h. Then the diameter of the barrier zone was measured and tabulated in millimetres.

Antioxidant activity

DPPH radical assay

The aqueous leaf extract of *Solanum nigrum*, Chem CuO-NPs and biosynthesized (10 ml) CuO-NPs were tested for the scavenging effect on DPPH (1,1-Diphenyl-2-Picry hydroxyl) radical methods, as reported in Das et al. [32]. Different concentrations of 15, 30, 60, 125, 250 and 500 µg/ml of the test sample solution were added to an equivalent volume of 0.1 mM methanolic DPBH solution. The reaction mixture was incubated for 60 min at room temperature. The optical intensity of the peak 517 nm was measured for the mixture, which gives the antioxidant activity. Ascorbic acid was as a standard to calibrate the resultant activity. The percentage of inhibition was calculated using the formula [33].

$$\%\ \text{DPPH scavenging activity} = \left(\frac{\text{Absorbance of control} - \text{absorbance of test sample}}{\text{Absorbance of control}}\right) \times 100. \tag{2}$$

Hydroxyl radical scavenging assay

Hydroxyl radical scavenging activities of aqueous leaf extract of *Solanum nigrum*, Chem CuO-NPs and biosynthesized (10 ml) CuO-NPs was measured using the deoxyribose method [34]. The reaction mixture contained 0.8 ml of phosphate buffer solution (50 m mol/l, PH 7.5), 0.2 ml of a sample of different concentrations 15, 30, 60, 125, 250 and 500 µg/ml, 0.2 ml of EDTA (1.04 m mol/l) 0.2 ml of $FeCl_3$ (1 m mol/l) and 0.2 ml of 2-deoxyribose (60 m mol/l). The mixture was placed in tubes, closed tightly and incubated at 37 °C for 15 min. the reaction was stopped by adding 0.2 ml of ascorbic acid (2 m mol/l) and 0.2 ml H_2O_2 (10 m mol/l). It was incubated at 37 °C for 1 h and then 2 ml of cold theobarbituric acid (10 g/l) was added to the reaction mixture. 2 ml of HCL (25%) was added to the above mixture. The mixture was heated at 100 °C for 15 min, the colour intensity of the green was formed and it was measured with a spectrophotometer and stabilized at 531 nm. The result was ascorbic acid as a standard for measuring activity. Scavenging percentage was calculated using the following formula [33]:

$$\% \text{ Hydroxyl radical scavenging} = [\text{Absorbance of the control} - (\text{Absorbance after adding sample} - \text{Absorbance sample with deoxyribose})] \times 100 / \text{Absorbance of the control.} \quad (3)$$

Results and discussion

The detailed study was carried out on biosynthesized CuO-NPs prepared using aqueous leaf extract of *Solanum nigrum* at various (5, 10, 15 and 20 ml) concentrations. Son et al. [35] performed the qualitative chemical test on *Solanum nigrum* leaf extract and established the presence of phytochemicals such as, flavonoids, saponins, alkaloids, proteins, glycosides, phenolic compounds, tannins, carbohydrates and fats. This phytochemicals initially reduces the metal ions and acts as stabling agent as well as in controlling the shape and size of the nanoparticles [36]. Flavonoids present in *Solanum nigrum* leaf extract can be release a reactive hydrogen atom, while tatutomeric changes are made from enol to keto by reducing copper nitrate to CuO-NPs [37].

UV–visible analysis

Optical absorption properties of the synthesized CuO-NPs are investigated by UV–visible spectroscopy. UV–visible spectra of samples exhibit a broad absorption peak in the range of 200–1200 nm as shown in Fig. 2a. The surface plasmon resonance (SPR) of the Chem CuO-NPs shows an excitonic absorption edge at 342 nm. The SPR peak of the biosynthesized CuO-NPs using *Solanum nigrum* leaf extract (5, 10, 15 and 20 ml) are shifted to 372, 383, 364 and 358 nm, respectively. The optical properties of metals oxides depend on the particle size switching to the SPR band wavelength [38]. The SPR absorption band at 383 nm indicates the good formation of biosynthesized (10 ml) CuO-NPs which are quite stable with no significant variance in the shape and size as reported earlier [39]. At minimum concentration of *Solanum nigrum* leaf extract (5 ml), no aggregation takes place due to its deficiency of biomolecules. The higher concentrations of (15 and 20 ml) show a significant effect on the synthesized CuO-NPs, here the more availability of phytochemicals would act as reducing, capping and stabilizing agent which stops the formation of nanoparticles aggregation [40]. The above result concludes that the optimised leaf extract concentration is 10 ml. The estimation of bandgap of synthesized CuO-NPs is done Tauc relation [2].

$$\alpha h\upsilon = A\,(h\upsilon - \text{Eg})^{1/2}, \quad (4)$$

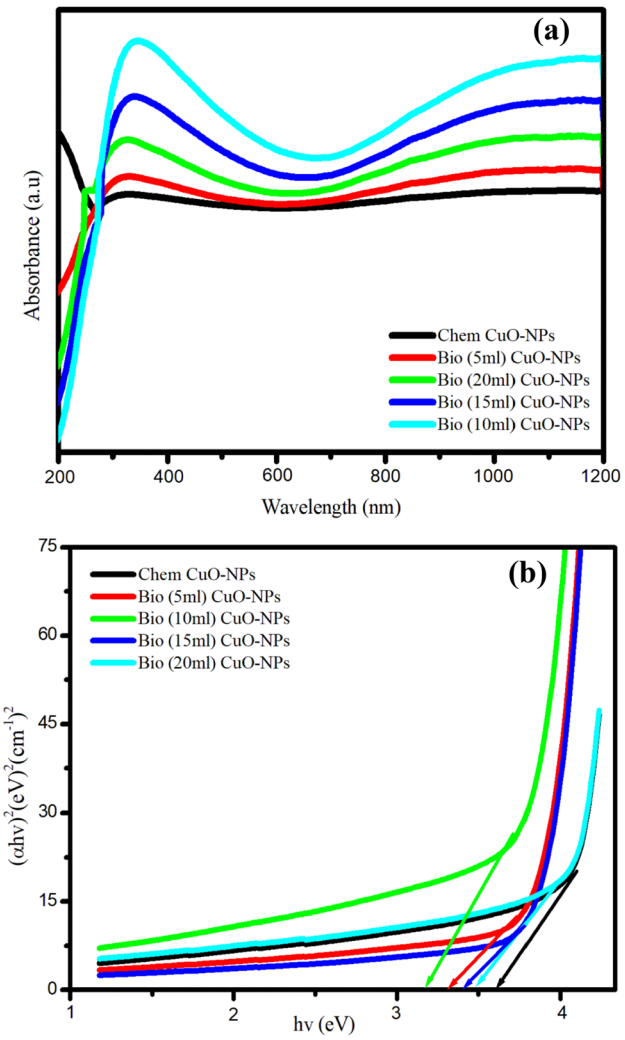

Fig. 2 **a** UV–Vis spectra of Chem CuO-NPs and biosynthesized (5, 10, 15 and 20 ml) CuO-NPs. **b** Optical bandgap enegry of Chem CuO-NPs and biosyntheiszed (5, 10, 15 and 20 ml) CuO-NPs

Table 1 Optical bandgap energy of Chem CuO-NPs and biosynthesized (5, 10, 15 and 20 ml) CuO-NPs

Samples	Band gap (eV)
Chem	3.63
Bio (5 ml)	3.33
Bio (10 ml)	3.24
Bio (15 ml)	3.41
Bio (20 ml)	3.46

where $h\upsilon$ is the photon energy (Js), α is the optical absorption coefficient (A/t) and A is energy independent constant, Eg is the direct bandgap (eV). Figure 2b shows the optical bandgap of Chem CuO-NPs and biosynthesized CuO-NPs, respectively, and the bandgap value calculated is listed in Table 1. From the table, confirms that biosynthesized CuO-NPs which is quite low compare to Chem CuO-NPs. The

bandgap energy decreases as the *Solanum nigrum* leaf extract is increased from 5 to 10 ml, and on further increase in the concentration of leaf extract to 15 and 20 ml, the optical bandgap energy is found to increased thereby confirming the decrease in the crystalline size of the sample for the concentrations, which could also be evidenced from XRD analysis [14]. The decrease in bandgap is due to fact that the crystal lattice is expanded and the interatomic bonds weakened with the increase of leaf extract concentration. The bond which easily breaks is called weaker bond and from that can get an electron to conduction band [41]. The biosynthesized (10 ml) CuO-NPs is highly effective and can significantly enhance photocatalytic and antibacterial application.

X-ray diffraction analysis

X-ray diffraction analysis is used to examine the crystal phases and crystallinity of the obtained CuO-NPs. Figure 3a represents the XRD pattern of Chem and biosynthesized CuO-NPs. The observed peaks corresponding to Miller indices (−110), (002), (111), (−202), (020), (202), (−113), (−311), (−220), (311) and (−222) confirms that monoclinic structure of CuO-NPs, which matched with the JCPDS card no: 45-0937. This type of results is obtained from leaf extract of *Lantana camara*-mediated CuO-NPs [3]. No impurity peaks other than CuO are observed in the XRD pattern indicating that all products have high phase purity. Moreover, the obtained diffraction reflections are well defined with high intensity, which clearly confirmed that the biosynthesized CuO-NPs are well crystalline. The biosynthesized CuO-NPs, the shift of angle (2θ) along major (002) and (111) diffraction planes as a function of phyotochemical present in the *Solanum nigrum* was observed. These data reveal that the positions of peaks slightly shifted toward the right side of the biosynthesized CuO-NPs compared to Chem CuO-NPs, on further increasing the leaf extract concentrations also the shift increase (Fig. 3b).

The crystallite size (D), dislocation density (δ) and microstrain (ε) of the samples were estimated using equation [2, 3];

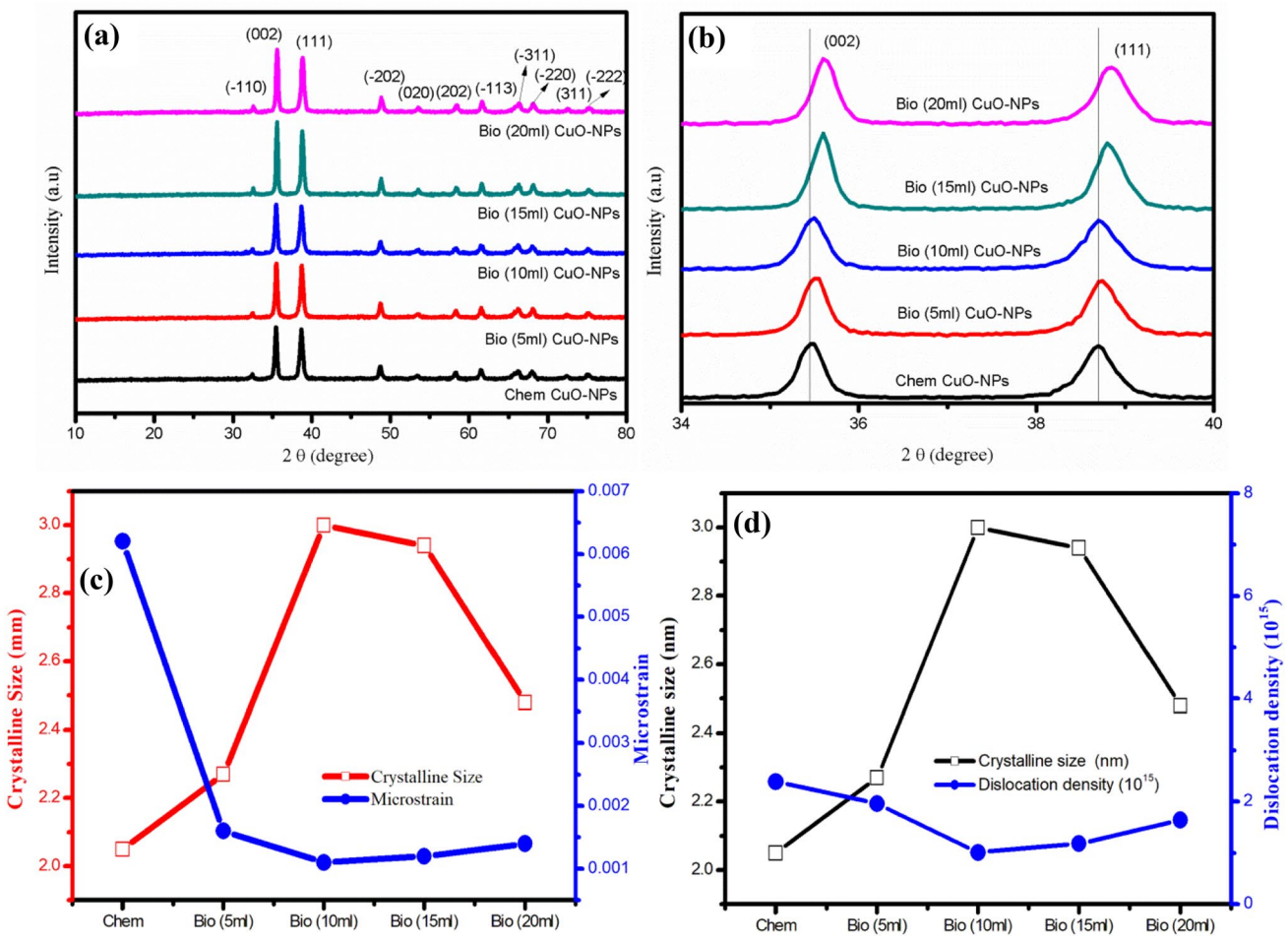

Fig. 3 **a** X-ray diffraction pattern; **b** the shift of peak position; **c, d** inter-relation between crystalline size, microstrain and dislocation of Chem CuO-NPs and biosynthesized (5, 10, 15 and 20 ml) CuO-NPs

$$D = \frac{0.9\lambda}{\beta \cos\theta}, \tag{5}$$

$$\delta = \frac{1}{D^2}, \tag{6}$$

$$\varepsilon = \frac{\beta \cos\theta}{4}, \tag{7}$$

where θ is Bragg angle, β is the full width at half maximum (FWHM), k is a shape factor ($k = 0.9$ in this work), λ is the wavelength of incident X-rays ($\lambda = 0.15406$ nm) and (hkl) are the Miller indices. The crystalline size of the Chem and biosynthesized CuO-NPs is ranged between 2.05 and 3.00 nm as shown in Tables 2 and 3. From the table, it is observed that the crystallite size of the particles increase with increase in the concentrations of *Solanum nigrum* leaf extract from 5 and 10 ml and with further increase in the concentrations to 15 and 20 ml, the crystallite size of the particles also decreases gradually. The crystallite size decreased and it confirmed the UV–visible spectral analysis. The minimum crystalline size was observed for biosynthesized (5 ml) CuO-NPs due to quantum confinement effect [33]. The obtained crystallite size from the biosynthesized (5 ml) is smaller from others leaf extract used to synthesize CuO-NPs [3, 42, 43] and *Solanum nigrum* leaf extract using biosynthesized Ag-NPs [29], Au-NPs [30], CeO_2-NPs [33] and ZnO-NPs [44]. The variation of crystalline size, microstrain and dislocation density for the Chem and biosynthesized CuO-NPs are shown in Fig. 3c, d. The microstrain is directly proportional to the dislocation density and inversely proportional to the crystalline size. The *Solanum nigrum* leaf extract strongly affects the structural parameters like, crystalline size, microstrain and dislocation density are shown in Fig. 3c-d and Table 3. The small dislocation density for biosynthesized CuO-NPs indicates higher crystallisation of the sample. Thus low concentration (5 ml) of biosynthesized CuO-NPs shows high level of surface defects and deteriorates crystal quality. But higher concentrations (10, 15 and 20 ml) of biosynthesized CuO-NPs show low level of surface defects.

Table 2 Structural parameter of Chem CuO-NPs and biosynthesized (5, 10, 15 and 20 ml) CuO-NPs

	2θ (°)	Miler indices (hkl)	D space	FWHM	Crystal size D (nm)	Microstrain (ε)	Dislocation density (δ) × 10^{15}
Chem	35.6024	002	2.51966	0.39660	2.20	0.0164	2.07
	38.8464	111	2.31639	0.51000	1.72	0.0020	3.36
	48.0619	− 202	2.36231	0.36620	2.24	0.0151	1.74
Bio (5 ml)	35.4295	002	2.53156	0.34520	2.52	0.0014	1.57
	38.6661	111	2.32978	0.41970	2.09	0.0017	2.28
	48.9837	− 202	1.86884	0.41260	2.21	0.0016	2.05
Bio (10 ml)	35.5067	002	2.56241	0.26790	3.25	0.0011	0.94
	38.7002	111	2.32481	0.29950	2.94	0.0012	1.16
	48.7876	− 202	1.86511	0.28060	3.25	0.0011	0.94
Bio (15 ml)	35.5733	002	2.51662	0.28010	3.11	0.0011	1.03
	38.7767	111	2.32040	0.32320	2.72	0.0013	1.35
	48.8275	− 202	1.86368	0.30980	2.94	0.0012	1.16
Bio (20 ml)	35.4687	002	2.52886	0.32480	2.68	0.0013	1.39
	38.6847	111	2.32570	0.36950	2.38	0.0015	1.77
	48.7412	− 202	1.86677	0.38250	2.38	0.0015	1.76

Table 3 Compared to the wavelength, bandgap and different structural parameter of Chem CuO-NPs and biosynthesized (5, 10, 15 and 20 ml) CuO-NPs

Samples	Wavelength (nm)	Bandgap energy (eV)	Average crystalline size (nm)	Average microstrain (ε)	Average dislocation density (δ) × 10^{15}
Chem	342	3.63	2.05	0.0062	2.39
Bio (5 ml)	372	3.33	2.27	0.0016	1.96
Bio (10 ml)	383	3.24	3.00	0.0011	1.01
Bio (15 ml)	364	3.41	2.94	0.0012	1.18
Bio (20 ml)	358	3.46	2.48	0.0014	1.64

DLS and ZP analysis

The zeta potential and particle size distribution of Chem and biosynthesized (10 ml) CuO-NPs are investigated by dynamic light scattering (DLS) technique uses to form hydrodynamic radius considering each particle as a separate sphere in Brownian movement [30]. The shell thickness of a capping or stabilizing agent consisting of metal nanoparticles is determined by DLS analysis. A fine range of particle size distribution is observed, average particle size is calculated for Chem CuO-NPs and biosynthesized CuO-NPs which are 78 and 55 nm, respectively and it is shown in Fig. 4a, b.

Zeta potential (ZP) values expose details regarding the surface area charge and also the stability of samples. Figure 4 (c-d) shows the average ZP values for Chem CuO-NPs and biosynthesized (10 ml) CuO-NPs are −3.14 and −27.12 mV, respectively. Since, ZP values above +30 eV or below −30 eV are high charge which makes repulsion between particles to prevent coalescence and aggregation of the nanoparticles [45]. The biosynthesized CuO-NPs have good stability and it is clear with the ZP value of −27.12 mV. The high negative value of ZP confirms that the capping particles present on the surface of CuO-NPs are comprised with negatively charged groups and charge of moderate stability of the nanoparticles. Flavonoids and protein present in the *Solanum nigrum* leaf extract could be reason for the reduction of metal ions and to stabilize the synthesized nanoparticles [30]. The observed zeta potential is analogous in previous study [43].

HR-TEM analysis

The shape, size and morphology of Chem CuO-NPs and biosynthesized (10 ml) CuO-NPs are using HR-TEM, which is represented by Figs. 5, 6. The HR-TEM images reveal that the particles have spherical morphology. The size distribution of Chem CuO-NPs and biosynthesized CuO-NPs exhibit the average size to be 32 and 25 nm as shown in Figs. 5f and 6f. A slight change in particle size and microstructure was observed in biosynthesized CuO-NPs when compared to Chem CuO-NPs. Small particle are aggregated and coated with a thin organic layer, which acts as a capping organic agent. This may well explain that, even at the macroscopic level, the nanoparticles show a good dispersion within the biodegradable aqueous solution [43]. Apart from this, 2 nm resolution studies of synthesized nanoparticles shows 0.24 and 0.27 nm '*d*' space, which states the crystalline nature of nanoparticles (Figs. 5b, 6b). The surface plot analyses of Chem CuO-NPs and biosynthesized CuO-NPs images are shown in Figs. 5d, e and 6d, e. The biosynthesized CuO-NPs have the highest porous nature, thereby favouring the absorption of more dye molecules, which in turn would improve the performance of photocatalyst. The SAED pattern of Chem CuO-NPs and biosynthesized CuO-NPs in Fig. 5c and 6c shows the reflection corresponding to the monoclinic structure, and very well match with the XRD analysis. The particle size of Chem and biosynthesized (10 ml) CuO-NPs is compared to the XRD, DLS and HR-TEM image as shown in Fig. 7. The particle size measured by DLS is slightly bigger compare to HR-TEM micrographs and this is due to the hydrodynamic radius [30].

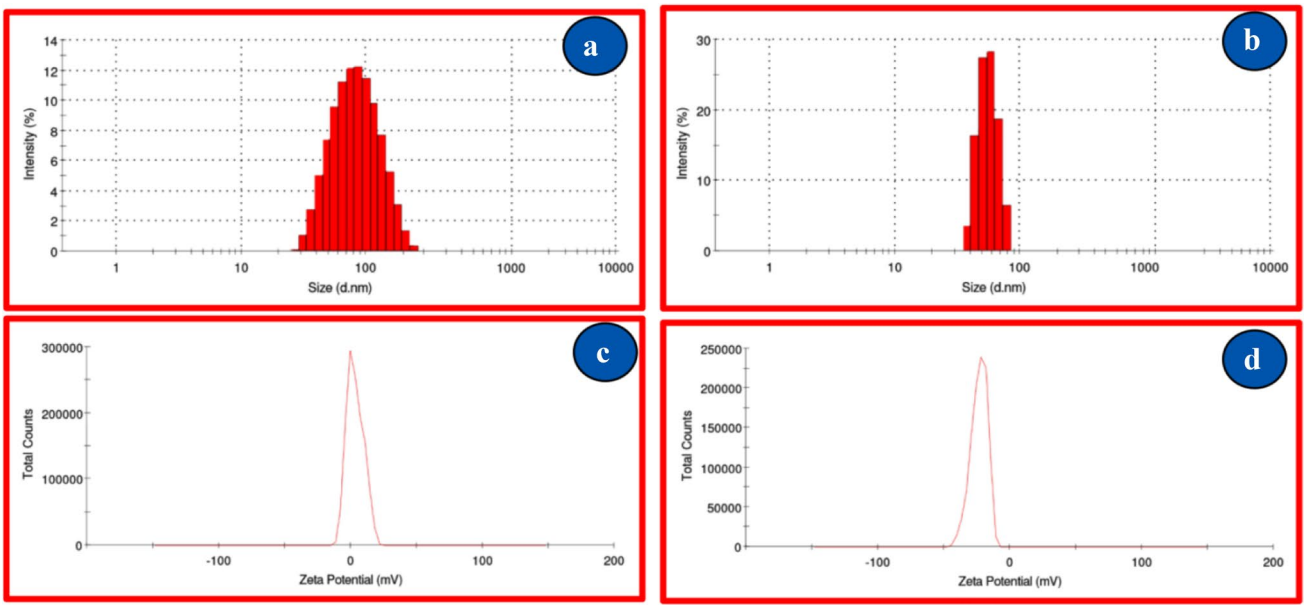

Fig. 4 **a, b** Dynamic light scattering pattern; **c, d** zeta potential distribution of Chem CuO-NPs and biosynthesized (10 ml) CuO-NPs

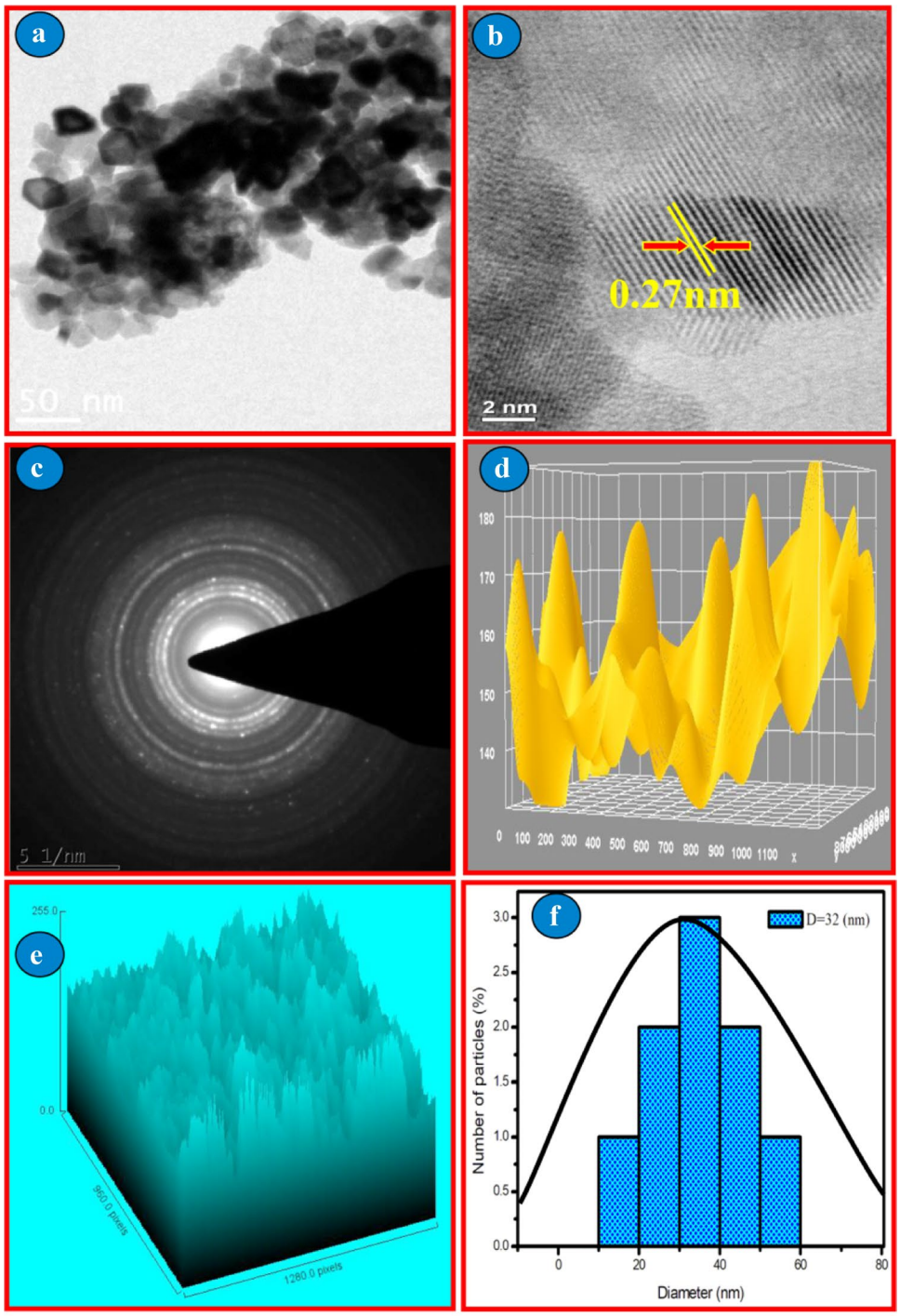

Fig. 5 **a** HR-TEM image; **b** lattice fringe; **c** SAED pattern; **d** particle size of Chem CuO-NPs

FT-IR analysis

Figure 8 present the FT-IR spectra of synthesized CuO-NPs and dried leaf extract of *Solanum nigrum*. The wave number and their corresponding functional group of the peaks are given in Table 4. The *Solanum nigrum* leaf extract show absorption peak at 3483.93, 2249.63, 1678.61 and 967.44 cm^{-1}. The peak at 3483.29 and 2249.63 cm^{-1} is corresponded to bending vibration-free O–H bonding and the presence of alkane C–H stretch [46]. The band around 1678.6 cm^{-1} can be assigned to the amide I and II N–H curves arising due to carbonyl stretching and peptide coupling of proteins, respectively. The band around 967.44 cm^{-1} may be corresponding to stretching or binding of the carboxylic acid [47]. From the FT-IR analysis, the presence of amides and carboxyl groups in the *Solanum nigrum* leaf extract is confirmed. The carboxyl functional groups are the main functional groups avail in the proteins, phenolic

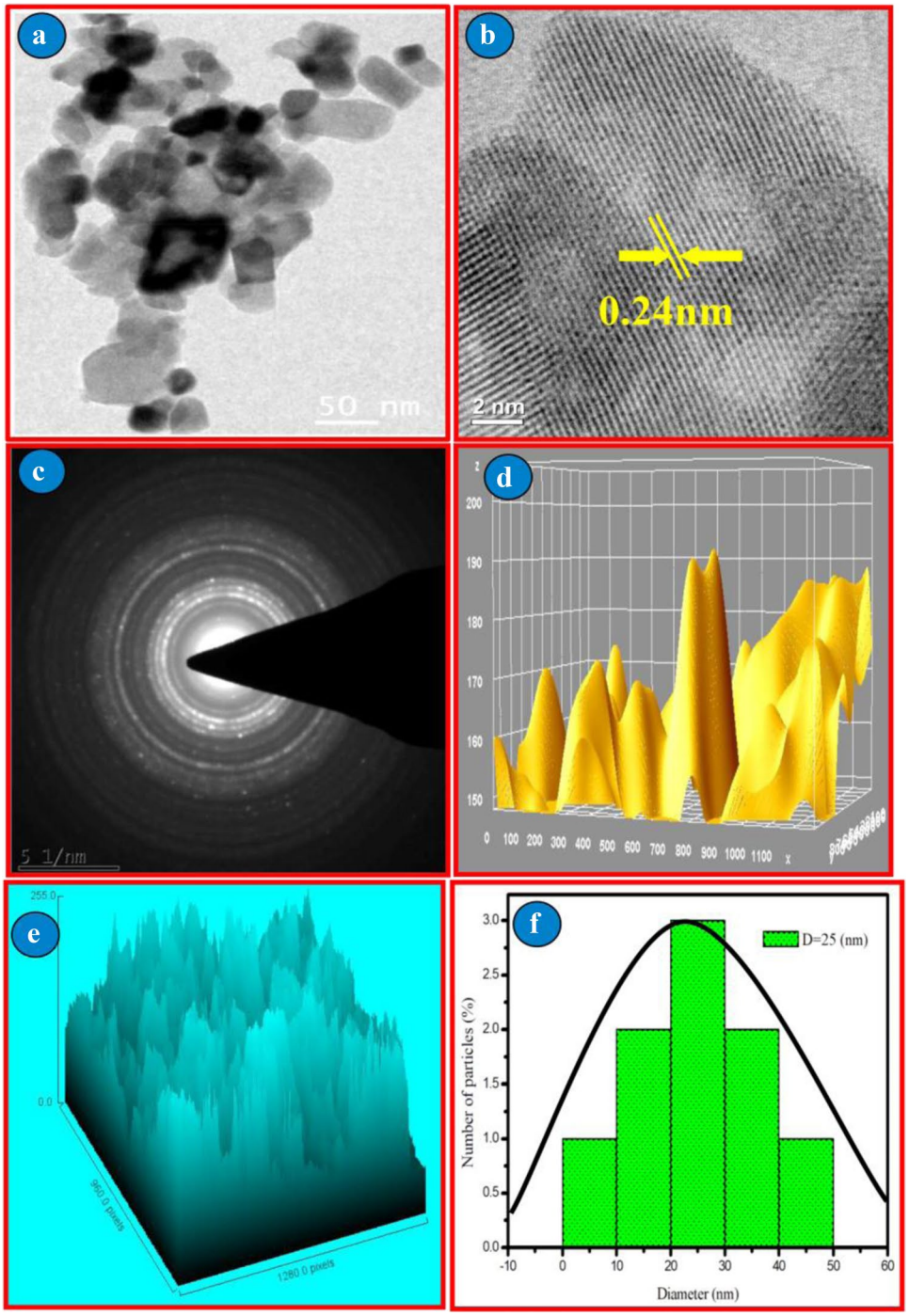

Fig. 6 **a** HR-TEM image; **b** lattice fringe; **c** SAED pattern; **d** particle size of biosynthesized (10 ml) CuO-NPs

compounds, flavonoids, vitamins, alkaloids, terpenes, tannins and saponin [35]. These phytochemicals are responsible for the bioreduction of copper nitrate into CuO-NPs.

The Chem CuO-NPs show absorption peak at 3414.26, 1489.21, 1072.94 and 849.12 cm^{-1}. The band around 1489.21 cm^{-1} confirms the deformation vibration of the C–H of alkane group. The bands around 1072.94 cm^{-1} is attributed OH bending vibration and C–H stretching, indicates the existence of a large number of hydroxyl groups [48]. The various concentrations (5, 10, 15 and 20 ml) of *Solanum nigrum* leaf extract using biosynthesized CuO-NPs for the FT-IR spectra show characteristic absorption bands around 3400–3450 cm^{-1}, 1600–1630 cm^{-1}, 1430–1450 cm^{-1}, 860–880 cm^{-1}, 590–620 cm^{-1} and 470–490 cm^{-1}. The bands around 3400–3450 cm^{-1} may be to C=O stretch of carboxylic acids [49]. The bands around 1430–1450 cm^{-1} are corresponding to aliphatic C–H bending and stretching vibrational modes. The bands around

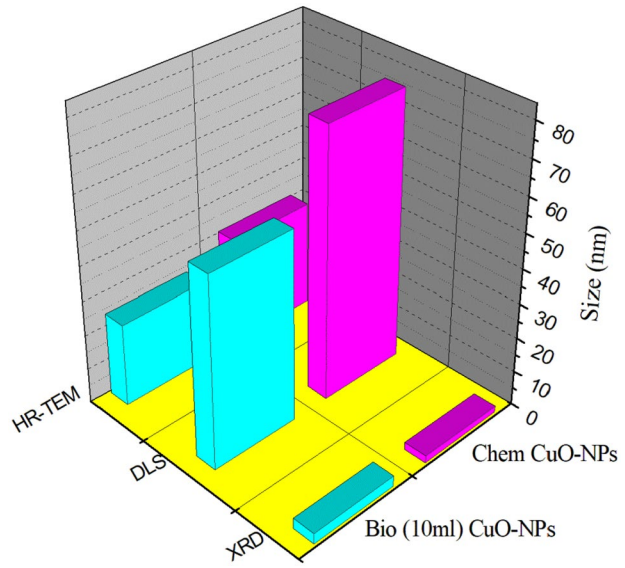

Fig. 7 Compared to size of XRD, DLS and HR-TEM Chem CuO-NPs and biosynthesized (10 ml) CuO-NPs

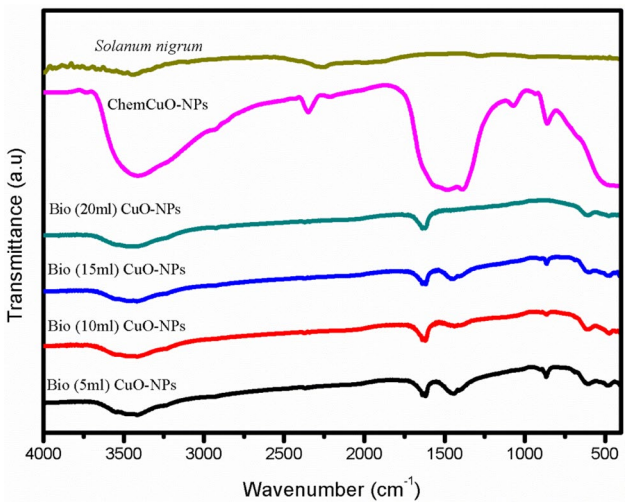

Fig. 8 FT-IR spectrum of *Solanum nigrum* leaf extract, Chem CuO-NPs and biosynthesized (5, 10, 15 and 20 ml) CuO-NPs

1600–1630 cm^{-1} may correspond to stretching vibrations of primary and secondary amines [50]. The band around 860–880 cm^{-1} can be assigned to the aromatic bending vibration of C–H group [51]. The two important characteristic bands appeared at 590–620 cm^{-1} and 470–490 cm^{-1} are assigned to the Cu–O stretching vibrational mode [52].

For biosynthesized CuO-NPs, important broadening of the spectral region is observed. An additional peak appeared around 1609 cm^{-1} is affecting the *Solanum nigrum* leaf extract. The relative intensity of observed peaks is increased with increasing concentrations of *Solanum nigrum* leaf extract which indicates the infrared analysis. The flavonoids in *Solanum nigrum* leaf extract are main reducing agents and this could be responsible for the reduction of copper nitrate. However, this peak is not present in the Chem CuO-NPs and some of the peak positions in biosynthesized CuO-NPs are slightly shifted. The shift is due to an interaction of *Solanum nigrum* leaf extract with CuO-NPs and solvent during biosynthesis.

Photoluminescence analysis

The photoluminescence (PL) spectra of Chem and biosynthesized CuO-NPs are shown in Fig. 9. The PL spectra have excitation wavelength of 325 nm. The PL spectra of synthesized CuO-NPs show two peaks located at 439 and 478 nm, respectively. The blue emission band at 439 nm is attributed to singly ionized Cu vacancies [53]. The blue-green emission band at 478 nm is due to surface defects in CuO-NPs associated with the transition between oxygen intermediate defects and oxygen vacancies. The PL spectra biosynthesized (5, 10, 15 and 20 ml) CuO-NPs values are 440–446 nm and 478–484 nm, respectively. When compared to Chem CuO-NPs, the red shift is observed for the biosynthesized CuO-NPs which may be from different origins like, localization of charge carriers, electron photon coupling due to lattice distortion, interface effects and point defects. The changes in the emission values confirm the *Solanum nigrum* leaf extract intermediated to CuO-NPs. Over all, it is clear that in Chem CuO-NPs, the cluster of electronic excitations occurs, which are not controlled by materials itself. In the biosynthesized CuO-NPs, the oxygen vacancies and defects which are present will bind the photoinduced electron easily forms excitons and indicates the decrease in PL intensity. The enhanced PL intensity and the good crystalline nature of biosynthesized CuO-NPs exhibit desirable properties for catalysis application.

Photocatalytic analysis

The photocatalytic activity is carried out by employing the Chem and biosynthesized (10 ml) CuO-NPs as photocatalyst inorder to study the degradation of aqueous solution of MB dye determined by open air sunlight. The catalytic degradation of dye is shown in Fig. 10a, b. UV–Vis spectra are recorded from 400 to 800 nm for various time intervals 0, 10, 20, 30, 40 and 50 min. The UV–Vis absorption peak at 663 nm refers to the MB dye, which is reduced to dark blue colour to colourless due to electron transfer. A band is observed at 663 nm indicating that 85 and 97% of the dyes are depleted in exactly 50 min, respectively, by the Chem CuO-NPs and biosynthesized CuO-NPs. The improved reduction rate by addition of the catalyst is because of the intermediate redox potential value between the acceptor and

Table 4 Functional group and commonly assigned component of *Solanum nigrum* leaf extract, Chem CuO-NPs and biosynthesized (5, 10, 15 and 20 ml) CeO_2-NPs

Wave number (cm^{-1})						Functional group and commonly assigned component
S. nigrum leaf extract	Chem CuO-NPs	Bio CuO-NPs				
		5 ml	10 ml	15 ml	20 ml	
3483.93	3414.26	3422.74	3415.96	3410.96	3407.14	free O–H bonding
2249.63	2206.53	–	–	–	–	C–H stretching
1678.61	–	1609.32	1622.48	1626.38	1629.06	C=O acid
–	1489.21	1439.85	1437.41	1453.01	–	C–C stretching vibrations
967.44	1072.94	–	–	–	–	C–O stretching mode of vibrations
–	849.12	862.47	855.74	868.36	–	C–O stretch
–	–	615.18	608.94	595.18	615.78	C–H vibrations
–	–	475.28	482.26	472.98	475.36	C=O stretch

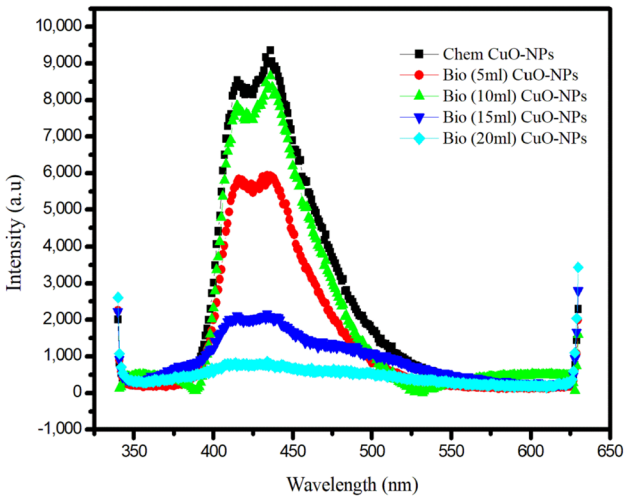

Fig. 9 Photoluminescence spectra of Chem CuO-NPs and biosynthesized (5, 10, 15 and 20 ml) CuO-NPs

donor through the electron transfer process [54]. Biosynthesized CuO-NPs perform as efficient redox catalyst due to its electron relay effect. Size of metal nanoparticles plays an important role in the catalytic reduction, while increase in the number of low coordinate copper atoms occurs with decrease in the size of biosynthesized CuO-NPs, which motivates the adsorption of the reactants on the catalyst surface and facilitates the degradation. Hence, increase in the surface area of the particles will significantly enhance the efficiency of the catalyst.

Mechanism of photocatalytic activity

The photocatalytic activities mainly vary with the oxygen vacancy variations. Based on the number of oxygen vacancies present, the electron–hole pairs are separated. The main advantage is that more oxygen vacancies would allow quick electron–hole recombination, which results in decreasing the photocatalytic activity for Chem CuO-NPs. According to Malleshappa et al. [55],based on the concentration of the defects at the surface level, the photocatalytic activity changes. The surface defects increase, particle size decreases and hence the charge carrier recombination rate increases which results in the increased photocatalytic activity. In the current study, biosynthesized CuO-NPs show lower particle sizes that illustrate high photocatalytic activity. This is due to the high efficiency of the separation of photogenerated charge carriers, improved light absorption and larger specific surface area.

Based on the results, possible mechanism (Fig. 11) for the MB dye photodegradation over synthesized nanoparticles irradiated in sunlight is projected according based on the reaction steps as given below [27]:

$$\mathrm{CuO} + \mathrm{h}\nu \rightarrow \mathrm{CuO}\left(\mathrm{e}^- + \mathrm{h}^+\right), \tag{8}$$

$$\mathrm{CuO}(\mathrm{h}^+) + \mathrm{OH}^- \rightarrow \mathrm{OH}^{\cdot}, \tag{9}$$

$$\mathrm{CuO}\left(\mathrm{e}^+\right) + \mathrm{O}_2 \rightarrow \mathrm{O}_2^{\cdot -}, \tag{10}$$

$$\mathrm{O}_2^{\cdot -} + \mathrm{H}^+ \rightarrow \mathrm{HO}^{2\cdot}, \tag{11}$$

$$\mathrm{CuO}\ (\mathrm{e}^-) + \mathrm{H}^+ + \mathrm{HO}_{2\cdot} \rightarrow \mathrm{OH}^{\cdot} + \mathrm{OH}^-, \tag{12}$$

$$\mathrm{O}_2^{\cdot -} + \mathrm{HO}_{2\cdot} + \mathrm{OH}^{\cdot} \text{ or } \left(\mathrm{h}^+\right) + \text{MB dye degradation product.} \tag{13}$$

From the reaction steps shown, when the biosynthesized CuO-NPs are irradiated with sunlight, the valence band (VB) is excited to the electron (e^-) conduction band (CB), while an equal number of holes are generated in the valence band (VB). To create OH^- radical species, photoinduced holes interact directly with MB dye. This is a strong oxidant for the mineralization of MB. To yield $O_2^{\cdot -}$,

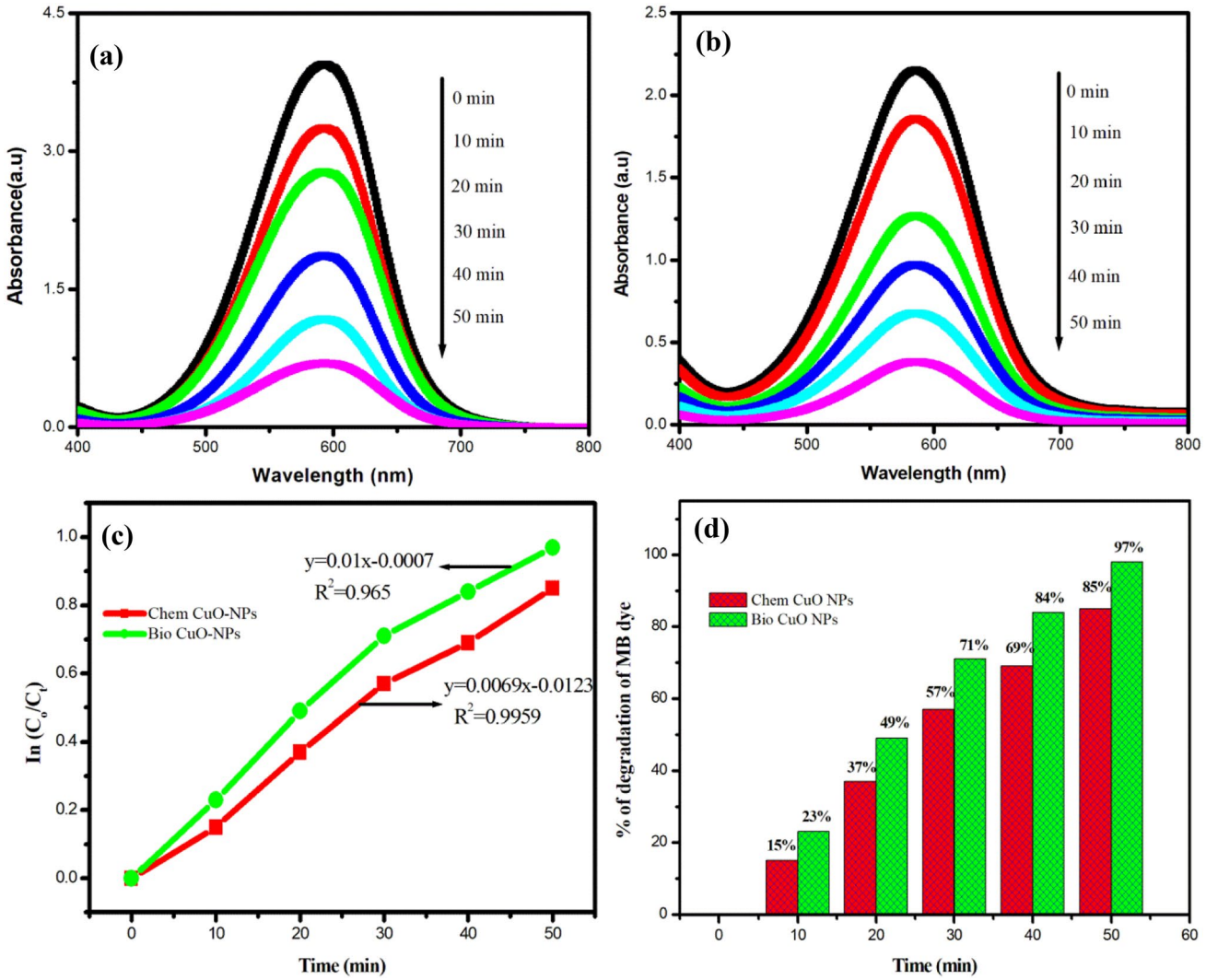

Fig. 10 **a, c** UV–Vis absorption spectra of MB with respect to irradiation time versus; **b, d** rate constant (K) and regression (R^2); **e** % degradation of MB dye compared to the Chem CuO-NPs and biosynthesized (10 ml) CuO-NPs

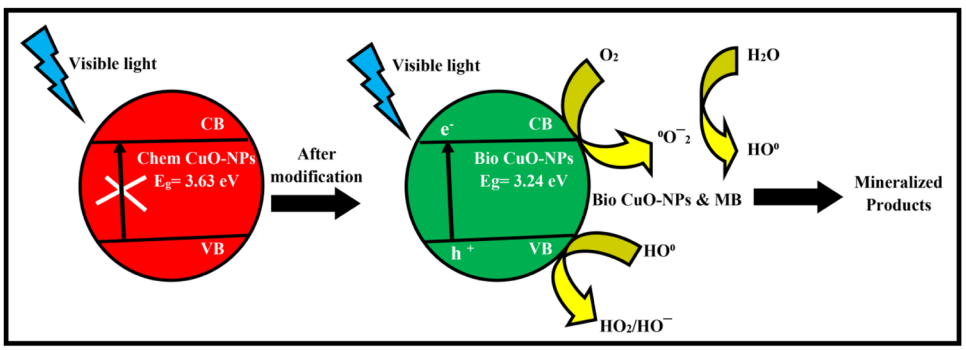

Fig. 11 Proposed mechanism for photodegradation of MB by synthesized CuO-NPs

the electron formation could react with adsorbed molecular oxygen's. Further, $O_2^{\cdot-}$ is combined with H^+ to produce HO_2• and this can react with the trapped electron to generate $OH^{\bullet}$ radical. Thus MB dye could be degraded by the produced reactive species are HO_2•, $OH^{\bullet}$ and $O_2^{\cdot-}$.

Kinetic studies

The pseudo first-order kinetics degradation of MB dye by photocatalysts is [33]:

$$\ln\left(C_0/C_t\right) = -kt, \tag{14}$$

where t is the reaction time (min), k is apparent reaction rate constant, C_0 is initial concentration of aqueous MB, and C is the concentration of aqueous MB at the reaction time of t (min). The kinetics of photodegradation of MB dye by Chem CuO-NPs and biosynthesized CuO-NPs are calculated and obtained results are shown in Fig. 10c. From the pseudo-first-order rate equation, the rate constant (K) for MB dye degradation by synthesized CuO-NPs is determined. The plot of In (C_0/C_t) as a function of irradiation time produces the rate constant values 0.0069 min^{-1}. Furthermore, the fitting correlation coefficient (R^2) is determined to be 0.9650. Biosynthesized CuO-NPs has rate constant value 0.01 min^{-1} and fitting correlation efficient (R^2) is determined as 0.9959. Finally, it is concluded that the C_0/C_t is decreased with increase of time and vice versa and the percentage of dye degradation is increased with increase of time and it is shown in Fig. 10d. According the result, the *Solanum nigrum* leaf extract using biosynthesized CuO-NPs shows better photocatalytic activity on MB dye compared to other plant extracts and the results are given in Table 5.

Antibacterial activity

The antibacterial activity of aqueous leaf extract of the *Solanum nigrum*, Chem and biosynthesized (10 ml) CuO-NPs is evaluated by measuring zone of inhibition (ZOI) with various concentrations (50 and 100 µl) against various pathogenic organisms. The antibacterial activity of samples is compared with two Gram-negative and two Gram-positive bacterial cultures such as, *B. subtilis*, *S. saprophyticus*, *E. coli* and *P. aeruginosa* in a different concentrations, as it is clearly shown in Fig. 12. The diameter of ZOI is given in Table 6. The aqueous leaf extracts of *Solanum nigrum* have highest inhibition zone and it is observed against *E. coli* (12 ± 0.1 nm), *B. subtilis* (11 ± 0.3 nm), *S. saprophyticus* (10 ± 0.2 nm) and *P. aeruginosa* (8 ± 0.5 nm) at concentration of 100 µl. In Chem CuO-NPs, highest inhibition zone is formed against *E. coli* (15 ± 0.4 nm), *B. subtilis* (13 ± 0.1 nm), *P. aeruginosa* (12 ± 0.6 nm) and *S. saprophyticus* (11 ± 0.2 nm) at concentration of 100 µl.

The biosynthesized CuO-NPs exhibit excellent antibacterial activity against all tested microorganisms. When compared to aqueous leaf extract of *Solanum nigrum* and Chem CuO-NPs at a concentration of 100 µl, maximum inhibition zone is observed against *E. coli* (21 ± 0.3 nm), *B. subtilis* (19 ± 0.5 nm), *S. saprophyticus* (18 ± 0.2 nm) and *P. aeruginosa* (18 ± 0.7 nm). From this result concentration of CuO-NPs, when they are extended the inhibition zone is also increased. Biosynthesized CuO-NPs have high inhibition zone against Gram positive and Gram negative in various concentrations when compare to aqueous leaf extract of *Solanum nigrum* and Chem CuO-NPs. The maximum antibacterial activity is observed by Gram-negative bacteria than the Gram-positive bacteria due to their cell structure. Both bacteria differ in their cell structure. A Gram-positive bacterium contains single thick cell wall which is made up of peptide glycan layer. It has very less toxicity due to thicker layers, whereas Gram-negative bacteria contains double thin layers cell which is made up of lip polysaccharide layer and it is followed by peptide glycan layer. The peptide glycan layer in Gram negative is thinner than the layer in Gram positive. The Gram-negative bacteria also has repeated unit of amino acids and carbohydrate [30]. Previous studies report that the interaction of CuO-NPs towards the *Solanum nigrum* leaf extract (phenolic and flavonoids) has high affinity for the bacterial cell surface, it binds to bacteria as a subsequent release of Cu ions cell membrane protein and DNA causes cell disruption membrane and DNA is damaged [57]. Due to the small particle size and large surface area of biosynthesized CuO-NPs, it exhibit an excellent antibacterial

Table 5 Comparison of phototcatalytic activity of CuO-NPs prepared from different plant extract

Materials used	Biological entity	pollutant	Degradation efficiency (%)	Time of degradation	References
CuO-NPs	Chemically	Methylene blue	85	50 min	Present work
CuO-NPs	*Solanum nigrum* leaf	Methylene blue	97	50 min	Present work
CuO-NPs	*Lemongrass* leaf	Methylene blue	80	300 min	[26]
CuO-NPs	*Aspergillus fumigates* leaf	Methylene blue	97	200 min	[24]
CuO-NPs	*Sida acuta* leaf	Methylene blue	93	100 min	[28]
CuO-NPs	*Solanum lycopersicum* leaf	Methylene blue	97	300 min	[39]
CuO-NPs	*Madhuca longifolia* leaf	Methylene blue	77	120 min	[25]
CuO-NPs	*Psidium guajava* leaf	Nile blue	93	120 min	[56]

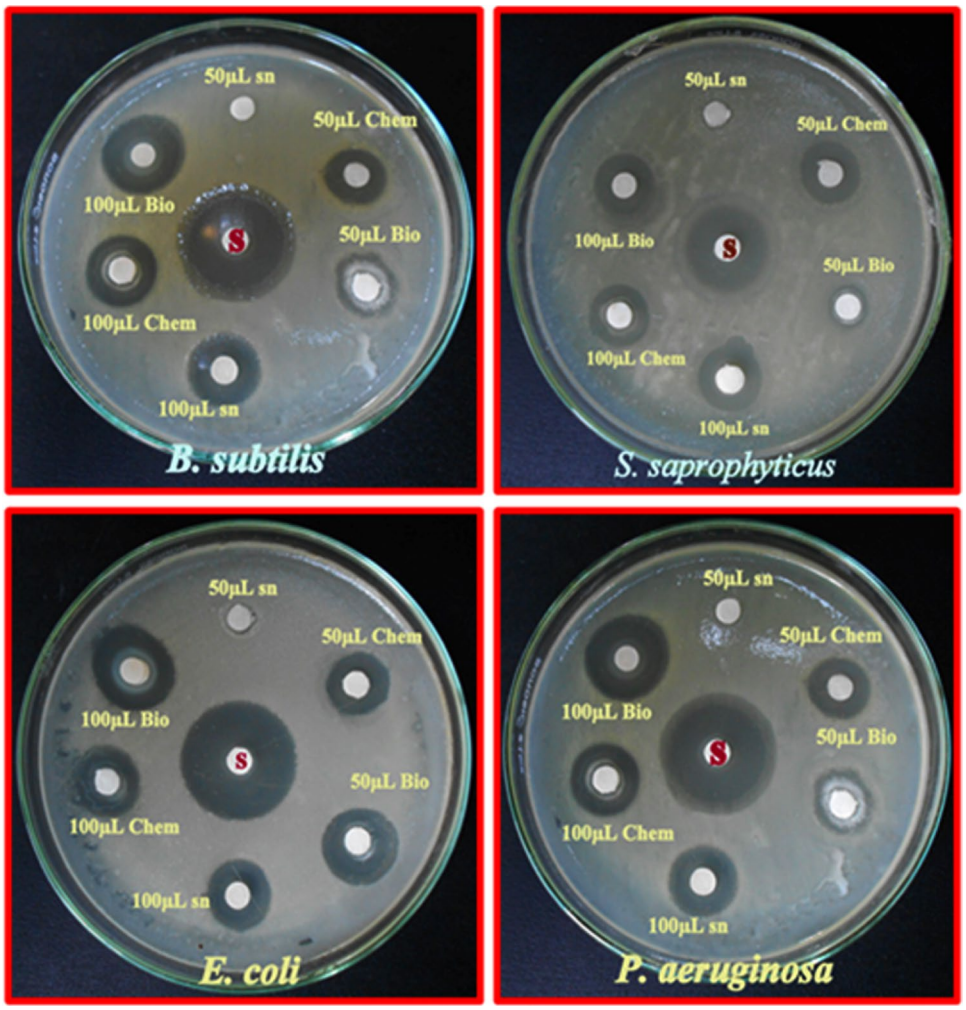

Fig. 12 Antibacterial activity of *Solanum nigrum* leaf extract, Chem CuO-NPs and biosynthesized (10 ml) CuO-NPs

Table 6 Antibacterial activity of *Solanum nigrum* leaf extract, Chem CuO-NPs, biosynthesized (10 ml) CuO-NPs and standard against human pathogenic bacteria

Bacteria	Zone of inhibition (mm)						Standard
	50 µl			100 µl			
	Chem CuO-NPs	*Solanum nigrum*	Bio CuO-NPs	Chem CuO-NPs	*Solanum nigrum*	Bio CuO-NPs	
B. subtilis	2	7	11	11	13	19	25
S. saprophyticus	2	8	6	10	11	18	25
E. coli	3	8	12	12	15	21	26
P. aeruginosa	1	6	9	8	12	18	25

activity compare to Chem CuO-NPs and *Solanum nigrum* leaf extract. Raghupathi et al. [58] have reported that small particle size is highly effective in inhibiting the growth of bacteria. Correlation between size of the particles and antibacterial activity is reported by Jeong et al. [59]. However, similar kind of antibacterial activity is proposed by Raja Naika et al. [28] and Arunkumar et al. [3]. Due to presence of terpenoids, tannins, flavonoids, alkaloids, carbodydrates, saponins, proteins and amino acids in *Solanum nigrum* leaf extract show potential bio-reducing and also bactericidal activity against the tested bacteria. This could be useful for biomedical applications.

Antioxidant activity

The antioxidant activity is one of the most important fundamental studies of nanomaterials [60]. Antioxidants play an important role in all living systems. In biological systems, free radicals are formed as a result interaction of biomolecules with molecular oxygen [61]. In the present

work, biosynthesized CuO-NPs show efficient antioxidant activity compare to Chem CuO-NPs due to their capping agent and it has great potential free radical. The present results are evident that the biosynthesized CuO-NPs not only have higher inhibitory action but also capping agent of the nanoparticles. The capping agents determine the surface charge and chemical properties of nanoparticles. They play an important role in free radical scavenging [62].

DPPH radical scavenging activity

DPPH is a standard nitrogen-concentrated free radical that is commonly used to relax the intensive scavenger function of compound or vegetation extraction. The standard DPPH intensity is reduced by the acceptance of hydrogen or electron [63]. The in vitro radical scavenging ability of the *Solanum nigrum* leaf extract, Chem CuO-NPs and biosynthesized (10 ml) CuO-NPs is evaluated by DPPH radical scavenging assays. Reduced activity of the samples was measured by changing the color of DPBH from the initial blue/purple solution to yellow, the solubility of the *Solanum nigrum* leaf extract, Chem CuO-NPs and biosynthesized CuO-NPs. The results of free radical scavenging activity at different concentrations (15, 30, 60, 125, 250 and 500 µg/ml) of samples are determined and compared with IC_{50} values with to the standard antioxidant ascorbic acid as shown in Fig. 13a.

At concentration 15–500 µg/ml, the *Soalnum nigrum* leaf extract shows scavenging rate ranging from 3 to 51%, Chem CuO-NPs show 9% to 62%, biosynthesized CuO-NPs show 19–90% and standard ascorbic acid show 28–95%. The above observed activity is lower than that of the standard vitamin C. Compare to the *Solanum nigrum* leaf extract, Chem CuO-NPs and biosynthesized CuO-NPs, ascorbic have the highest radical scavenging activity with the lowest IC_{50} µg/ml (125.34). *Solanum nigrum* leaf extract has the lowest radical scavenging activity with the highest IC_{50} µg/ml (189.12), Chem CuO-NPs show IC_{50} µg/ml (163.97) and biosynthesized CuO-NPs show moderated scavenging activity with IC_{50} µg/ml (131.54). The lower IC_{50} µg/ml values reflect the greater potency for antioxidant activity of the sample. The results for DPPH free radical scavenging activity (IC_{50} µg/ml) of *Solanum nigrum* leaf extract, Chem CuO-NPs, biosynthesized CuO-NPs and standard, produced by different concentrations, are presented in Table 7a.

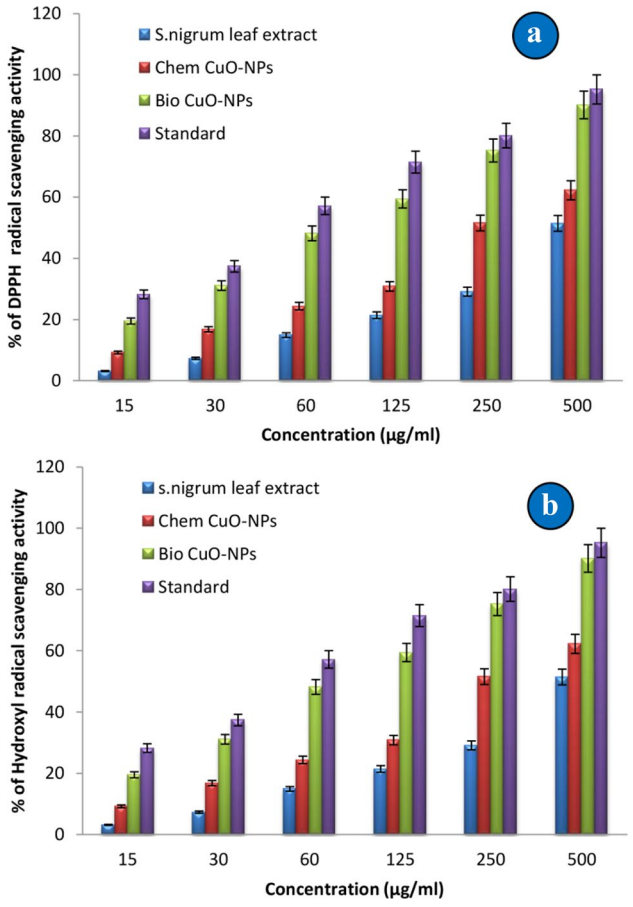

Fig. 13 **a** DPPH free radical; **b** hygroxyl radical scavenging assay of *Solanum nigrum* leaf extract, Chem CuO-NPs and biosynthesized (10 ml) CuO-NPs

Table 7 (a) DPPH free radical scavenging activity *Solanum nigrum* leaf extract, Chem CuO-NPs, biosynthesized (10 ml) CuO-NPs and ascorbic acid (standard), **(b)** hydroxyls radical scavenging activity of *Solanum nigrum* leaf extract, Chem CuO-NPs, biosynthesized (10 ml) CuO-NPs and ascorbic acid (standard)

Concentrations (µg/ml)	*S. nigrum* leaf extract	Chem CuO-NPs	Bio CuO-NPs	Standard
(a)				
500	51 ± 23	62 ± 13	90 ± 10	95 ± 31
250	29 ± 92	51 ± 42	75 ± 30	80 ± 52
125	21 ± 13	30 ± 40	59 ± 12	71 ± 83
60	14 ± 34	24 ± 42	48 ± 19	57 ± 15
30	7 ± 01	16 ± 19	31 ± 92	37 ± 76
15	3 ± 12	9 ± 82	19 ± 34	28 ± 34
IC_{50}	189.12	163.97	131.54	124.34
(b)				
500	51 ± 43	72 ± 24	93 ± 13	97 ± 21
250	30 ± 12	52 ± 54	77 ± 24	82 ± 13
125	21 ± 43	46 ± 83	61 ± 42	68 ± 45
60	15 ± 19	31 ± 38	49 ± 19	55 ± 17
30	8 ± 13	17 ± 18	28 ± 10	35 ± 38
15	4 ± 12	9 ± 21	17 ± 15	20 ± 23
IC_{50}	184.13	159.34	129.42	119.92

Hydroxyl radical scavenging activity

Hydroxyl radical can be generated by the Fenton reaction in the presence of reduced intermediate metals and H_2O_2, known as the major active oxygen species that causes lipid peroxide and enormous biological damage. Scavenging $OH^{\cdot}$ is an important antioxidant activity. Because of their reactivity, $OH^{\cdot}$ reacts with many molecules found in living cells, such as amino acids, sugars, lipids and nucleotides [64] and removes $OH^{\cdot}$ which is very important for the protection of living systems. The $OH^{\cdot}$ scavenging potential of various solvents of, *Solanum nigrum* leaf extract, Chem CuO-NPs and biosynthesized (10 ml) CuO-NPs are shown in Fig. 13b. The concentrations at 15–500 µg/ml inhibitions are found to be 4–54% for *Solanum nigrum* leaf extract, 9–72% for Chem CuO-NPs, 17–93% for biosynthesized CuO-NPs and 20 to 97% for Vitamin C. Compared to the *Solanum nigrum* leaf extract, Chem CuO-NPs and biosynthesized CuO-NPs, ascorbic have the highest radical scavenging activity with the lowest IC_{50} µg/ml (129.34). *Solanum nigrum* leaf extract has the lowest radical scavenging activity with highest IC_{50} µg/ml (184.13), Chem CuO-NPs show IC_{50} µg/ml (159.34) and biosynthesized CuO-NPs show moderated scavenging activity with IC_{50} µg/ml (135.42). The results for hydroxyl free radical scavenging activity (IC_{50} µg/ml) of *Solanum nigrum* leaf extract, Chem CuO-NPs, biosynthesized CuO-NPs and standard, produced by different concentrations, are presented in Table 7b. The lower IC_{50} values greater the hydrogen-donating ability and thus the antioxidant activity of the free radical scavengers [61]. CuO-NPs synthesized, characterization and antioxidant activity, is reported by Ghung et al. [65], Liaz et al. [66] and Rajeshkumar et al. [67]. The above results show that *Solanum nigrum* leaf extract is a good source of phenolic compounds and flavonoids. The flavonoids and phenolic have been reported to be the most important phytochemical responsible for antioxidant activity [68]. In this work, the CuO-NPs synthesized using leaf extract of *Solanum nigrum* show antioxidant activity due to capped phenolic compounds. The phenolic group facilitates the conversion of copper nitrate to CuO-NPs due to be electron donating ability.

Conclusion

Biosynthesis of nanoparticles offered an attractive alternate to chemical synthesis methods. *Solanum nigrum* leaf aqueous extract was utilized in the synthesis of metal and metal oxide nanoparticles. The optical bandgap of chemical and biosynthesized CuO-NPs was found to vary from 3.63 to 3.24 eV. XRD pattern exhibited the monoclinic structure of the synthesized CuO-NPs. Spherical-shaped morphology was found for chemical and biosynthesized CuO-NPs and it was confirmed by HR-TEM. The higher negative zeta potential value indicates better stability of biosynthesized CuO-NPs. The FT-IR studies revealed that the reducing CuO-NPs by flavonoids and phenols become helpful in capping and stabilization of particles. The small crystallite size of biosynthesized CuO-NPs had significant catalytic performance because of their high surface volume ratio and provided active sites of the reactant molecules to interact. The antibacterial and antioxidant were studies on chemical and biosynthesized CuO-NPs and confirmed that the biosynthesized CuO-NPs possessed an enhanced antibacterial activity against for Gram-negative and Gram-positive bacterial strain and also a strong DPPH radical antioxidant effect. Thus, it is concluded that biosynthesized CuO-NPs are more efficient, nontoxic and eco-friendly. They elicit their future treatment of polluted water bodies with dyes and also promising candidate for many medical applications.

Funding This research did not receive any specific grant from funding agencies in the public, commercial, or not-for-profit sectors.

Compliance with ethical standards

Conflict of interest The authors declare no conflict of interest.

References

1. Linic S, Aslam U, Boerigter C, Morabito M (2015) Photochemical transformations on plasmonic metal nanoparticles. Nat Mater 14:567–576
2. Muthuvel A, Jothibas M, Manoharan C (2020) Effect of chemically synthesis compared to biosynthesized ZnO-NPs using *Solanum nigrum* leaf extract and their photocatalytic, antibacterial and in-vitro antioxidant activity. J Environ Chem Eng 8:103705
3. Arunkumar B, Johnson Jeyakumar S, Jothibas M (2019) A sol-gel approach to the synthesis of CuO nanoparticles using *Lantana camara* leaf extract and their photo catalytic activity. Optik 183:698–705
4. Vinothkumar P, Manoharan C, Shanmugapriya B, Bououdina M (2019) Effect of reaction time on structural, morphological, optical and photocatalytic properties of copper oxide (CuO) nanostructures. J Mater Sci Mater El 30:6249–6262
5. Rafique M, Shafiq F, Ali Gillani SS, Shakil M, Tahir MB, Sadaf I (2019) Eco-friendly green and biosynthesis of copper oxide nanoparticles using *Citrofortunella microcarpa* leaves extract for efficient photocatalytic degradation of Rhodamin B dye form textile wastewater. Optik. https://doi.org/10.1016/j.ijleo.2019.164053
6. Tahir MB (2019) Microbial photoelectrochemical cell for improved hydrogen evolution using nickel ferrite incorporated WO_3 under visible light irradiation. Int J Hydrog Energy 44:17316–17322
7. Ahmad R, Mondal PK (2012) Adsorption and photodegradation of methylene blue by using PAni/TiO_2 nanocomposite. J Disper Sci Technol 33:380–386
8. Ahmad R, Kumar R (2011) Synthesis and properties of cellulose carbon encapsulated ZnO for dye removal. J Disper Sci Technol 32:737–740

9. Tahir MB, Kiran H, Iqbal T (2019) The detoxification of heavy metals from aqueous environment using nano-photocatalysis approach: a review. Environ Sci Pollut 26:10515–10528
10. Kumar R, Mondal PK, Ahmad R (2014) Adsorptive removal of hazardous methylene blue by fruit shell of *Cocos nucifera*. Environ Eng Manag J 13:231–240
11. Tahir MB, Nabi G, Rafique M, Khalid NR (2017) Nanostructured-based WO_3 photocatalysts: recent development, activity enhancement, perspectives and applications for wastewater treatment. Int J Environ Sci Tech 14:2519–2542
12. Bilal Tahir M, Nabi G, Rafique M, Khalid NR (2018) Role of fullerene to improve the WO_3 performance for photocatalytic applications and hydrogen evolution. Int J Energy Res 42:4783–4789
13. Bilal Tahir M, Nadeem Riaz K, Asiri AM (2019) Boosting the performance of visible light-driven WO3/g-C3N4 anchored with BiVO4 nanoparticles for photocatalytic hydrogen evolution. Int J Energy Res 43:5747–5758
14. Dorner L, Cancellieri C, Rheingans B, Walter M, Kagi R, Schmutz P, Kovalenko MV, Jeurgens LPH (2019) Cost-effective sol-gel synthesis of porous CuO nanoparticle aggregates with tunable specific surface area. Sci Rep 9:1
15. Khan A, Rashid A, Younas R, Chong R (2015) A chemical reduction approach to the synthesis of copper nanoparticles. Int Nano Lett 6:21–26
16. Phiwdang K, Suphankij S, Mekprasart W, Pecharapa W (2013) Synthesis of CuO nanoparticles by precipitation method using different precursors. Energy Proc 34:740–745
17. Felix S, Chakkravarthy RBP, Grace AN (2015) Microwave assisted synthesis of copper oxide and its application in electrochemical sensing. IOP Conf Ser Mater Sci Eng 73:012115
18. Rani P, Siril PF, Srivastava R (2017) Cu nanoparticles decorated Cu organic framework based efficient and reusable heterogeneous catalyst for coupling reactions. Mol Catal 433:100–110
19. Singh J, Dutta T, Kim K-H, Rawat M, Samddar P, Kumar P (2018) Green synthesis of metals and their oxide nanoparticles: applications for environmental remediation. J Nanobiotechnol 16:1
20. Jayakumarai G, Gokulpriya C, Sudhapriya R, Sharmila G, Muthukumaran C (2015) Phytofabrication and characterization of monodisperse copper oxide nanoparticles using *Albizia lebbeck* leaf extract. Appl Nanosci 5:1017–1021
21. Nasrollahzadeh M, Sajadi SM, Khalaj M (2014) Green synthesis of copper nanoparticles using aqueous extract of the leaves of *Euphorbia esula* L and their catalytic activity for ligand-free Ullmann-coupling reaction and reduction of 4-nitrophenol. RSC Adv 4:47313–47318
22. Abboud Y, Saffaj T, Chagraoui A, El Bouari A, Brouzi K, Tanane O, Ihssane B (2013) Biosynthesis, characterization and antimicrobial activity of copper oxide nanoparticles (CONPs) produced using brown alga extract (*Bifurcaria bifurcata*). Appl Nanosci 4:571–576
23. Sebeia N, Jabli M, Ghith A (2019) Biological synthesis of copper nanoparticles, using *Nerium oleander* leaves extract: characterization and study of their interaction with organic dyes. Inorg Chem Commun 105:36–46
24. Ghareib M, Abdallah W, Abu Tahon M, Tallima A (2019) Biosynthesis of copper oxide nanoparticles using the preformed biomass of *aspergillus fumigatus* and their antibacterial and photocatalytic activities. Dig J Nanomater Bios 14(2019):291–303
25. Das P, Ghosh S, Ghosh R, Dam S, Baskey M (2018) *Madhuca longifolia* plant mediated green synthesis of cupric oxide nanoparticles: a promising environmentally sustainable material for waste water treatment and efficient antibacterial agent. J Photochem Photobiol B 189:66–73
26. Hai Le Tu (2019) Biosynthesis, characterization and photocatalytic activity of copper/copper oxide nanoparticles produced using aqueous extract of *Lemongrass Leaf*. Compos Mater 3:30–35
27. Sathiyavimal S, Vasantharaj S, Bharathi D, Saravanan M, Manikandan E, Kumar SS, Pugazhendhi A (2018) Biogenesis of copper oxide nanoparticles (CuONPs) using *Sida acuta* and their incorporation over cotton fabrics to prevent the pathogenicity of Gram negative and Gram positive bacteria. J Photochem Photobiol B 188:126–134
28. Naika HR, Lingaraju K, Manjunath K, Kumar D, Nagaraju G, Suresh D, Nagabhushana H (2015) Green synthesis of CuO nanoparticles using *Gloriosa superba* L. extract and their antibacterial activity. J Taibah Univ Sci 9:7–12
29. Sengottaiyan A, Aravinthan A, Sudhakar C, Selvam K, Srinivasan P, Govarthanan M, Manoharan K, Selvankumar T (2015) Synthesis and characterization of *Solanum nigrum*-mediated silver nanoparticles and its protective effect on alloxan-induced diabetic rats. J Nanostruct Chem 6:41–48
30. Muthuvel A, Adavallan K, Balamurugan K, Krishnakumar N (2014) Biosynthesis of gold nanoparticles using *Solanum nigrum* leaf extract and screening their free radical scavenging and antibacterial properties. Biomed Prev Nutr 4:325–332
31. Suganya S, Jothibas M, Muthuvel A (2019) Effect of temperature on different properties of ZnS nanoparticles synthesized by solid-state reaction method. J Nanosci Nanotechnol 4:787–790
32. Das D, Nath BC, Phukon P, Kalita A, Dolui SK (2013) Synthesis of ZnO nanoparticles and evaluation of antioxidant and cytotoxic activity. Colloid Surf B 111:556–560
33. Muthuvel A, Jothibas M, Manoharan C, Jayakumar SJ (2020) Synthesis of CeO2-NPs by chemical and biological methods and their photocatalytic, antibacterial and in vitro antioxidant activity. Res Chem Intermediat 46:2705–2729
34. Loganayaki N, Siddhuraju P, Manian S (2011) Antioxidant activity and free radical scavenging capacity of phenolic extracts from *Helicteres isora* L. and *Ceiba pentandra* L. J Food Sci Tech 50:687–695
35. Son H, Yen P (2014) Preliminary phytochemical screening, acute oral toxicity and anticonvulsant activity of the berries of *Solanum nigrum* Linn. Trop J Pharm Res 13:907
36. Din MI, Arshad F, Hussain Z, Mukhtar M (2017) Green adeptness in the synthesis and stabilization of copper nanoparticles: catalytic, antibacterial, cytotoxicity, and antioxidant activities. Nanoscale Res Lett 12:1
37. Jacobs H, Moalin M, Bast A, van der Vijgh WJF, Haenen GRMM (2010) An Essential Difference between the Flavonoids Mono-HER and quercetin in their interplay with the endogenous antioxidant network. PLoS ONE 5:e13880
38. Gharibshahi E, Saion E (2012) Influence of dose on particle size and optical properties of colloidal platinum nanoparticles. Int J Mol 13:14723–14741
39. Vaidehi D, Bhuvaneshwari V, Bharathi D, Sheetal BP (2018) Antibacterial and photocatalytic activity of copper oxide nanoparticles synthesized using *Solanum lycopersicum* leaf extract. Mater Res Express 8:085403
40. Priya RS, Geetha D, Ramesh PS (2016) Antioxidant activity of chemically synthesized AgNPs and biosynthesized *Pongamia pinnata* leaf extract mediated AgNPs—a comparative study. Ecotox Environ Safe 134:308–318
41. Thurner C, Debbage P (2018) Molecular imaging with nanoparticles: the dwarf actors revisited 10 years later. Histochem Cell Biol 150:733–794
42. Narasaiah P, Mandal BK, Sarada NC (2017) Biosynthesis of copper Oxide nanoparticles from *Drypetes sepiaria* Leaf extract and their catalytic activity to dye degradation. IOP Conf Ser Mater Sci Eng 263:022012

43. Chand Mali S, Raj S, Trivedi R (2019) Biosynthesis of copper oxide nanoparticles using Enicostemma axillare (Lam.) leaf extract. B B Rep 20:100699
44. Ramesh M, Anbuvannan M, Viruthagiri G (2015) Green synthesis of ZnO nanoparticles using *Solanum nigrum* leaf extract and their antibacterial activity. Spectrochim Acta A 136:864–870
45. Senthilkumar N, Nandhakumar E, Priya P, Soni D, Vimalan M, Vetha Potheher I (2017) Synthesis of ZnO nanoparticles using leaf extract of *Tectona grandis* (L.) and their anti-bacterial, anti-arthritic, anti-oxidant and in vitro cytotoxicity activities. New J Chem 41:10347–10356
46. Ihsan M, Niaz A, Rahim A, Zaman MI, Arain MB, Sirajuddin S, Sharif T, Najeeb M (2015) Biologically synthesized silver nanoparticle-based colorimetric sensor for the selective detection of Zn^{2+}. RSC Adv 5:91158–91165
47. Handago DT, Zereffa EA, Gonfa BA (2019) Effects of *Azadirachta Indica* leaf extract, capping agents, on the synthesis of pure and Cu doped ZnO nanoparticles: a green approach and microbial activity. Open Chem 17:246–253
48. Knop S, Jansen TLC, Lindner J, Vohringer P (2011) On the nature of OH-stretching vibrations in hydrogen-bonded chains: pump frequency dependent vibrational lifetime. Phys Chem Chem Phys 13:4641
49. Jadhav MS, Kulkarni S, Raikar P, Barretto DA, Vootla SK, Raikar US (2018) Green biosynthesis of CuO & Ag–CuO nanoparticles from *Malus domestica* leaf extract and evaluation of antibacterial, antioxidant and DNA cleavage activities. New J Chem 42:204–213
50. Cuevas R, Duran N, Diez MC, Tortella GR, Rubilar O (2015) Extracellular biosynthesis of copper and copper oxide nanoparticles by *Stereum hirsutum*, a native White-Rot fungus from Chilean forests. J Nanomater 2015:1–7
51. Saif S, Tahir A, Asim T, Chen Y (2016) Plant Mediated green synthesis of CuO nanoparticles: comparison of toxicity of engineered and plant mediated CuO nanoparticles towards *Daphnia magna*. Nanomater 6:205
52. Anwaar S, Maqbool Q, Jabeen N, Nazar M, Abbas F, Nawaz B, Hussain T, Hussain SZ (2016) The effect of green synthesized CuO nanoparticles on callogenesis and regeneration of *Oryza sativa* L. Front Plant Sci. https://doi.org/10.3389/fpls.2016.01330
53. Dagher S, Haik Y, Ayesh AI, Tit N (2014) Synthesis and optical properties of colloidal CuO nanoparticles. J Lumin 151:149–154
54. Thammavongsy Z, Mercer IP, Yang JY (2019) Promoting proton coupled electron transfer in redox catalysts through molecular design. Chem Comm 55:10342–10358
55. Malleshappa J, Nagabhushana H, Sharma SC, Vidya YS, Anantharaju KS, Prashantha SC, Prasad BD, Naika HR, Lingaraju K, Surendra BS (2015) *Leucas aspera* mediated multifunctional CeO_2 nanoparticles: structural, photoluminescent, photocatalytic and antibacterial properties. Spectrochim Acta A 149:452–462
56. Das P, Ghosh S, Ghosh R, Dam S, Baskey M (2018) Madhuca longifolia plant mediated green synthesis of cupric oxide nanoparticles: a promising environmentally sustainable material for waste water treatment and efficient antibacterial agent. J Photochem Photobiol B 89:66–73
57. Slavin YN, Asnis J, Hafeli UO, Bach H (2017) Metal nanoparticles: understanding the mechanisms behind antibacterial activity. J Nanobiotechnol 15:1
58. Raghupathi KR, Koodali RT, Manna AC (2011) size-dependent bacterial growth inhibition and mechanism of antibacterial activity of zinc oxide nanoparticles. Langmuir 27:4020–4028
59. Jeong Y, Lim DW, Choi J (2014) Assessment of size-dependent antimicrobial and cytotoxic properties of silver nanoparticles. Adv Mater Sci Eng 2014:1–6
60. Jeevanandam J, Barhoum A, Chan YS, Dufresne A, Danquah MK (2018) Review on nanoparticles and nanostructured materials: history, sources, toxicity and regulations. Beilstein J Nanotechol 9:1050–1074
61. Lobo V, Patil A, Phatak A, Chandra N (2010) Free radicals, antioxidants and functional foods: impact on human health. Pharmacogn Rev 4:118
62. Shanmugam C, Sivasubramanian G, Parthasarathi B, Baskaran K, Balachander R, Parameswaran VR (2015) Antimicrobial, free radical scavenging activities and catalytic oxidation of benzyl alcohol by nano-silver synthesized from the leaf extract of *Aristolochia indica* L.: a promenade towards sustainability. Appl Nanosci 6:711–723
63. Fang M, Chen J, Xu X, Yang P, Hildebrand H (2006) Antibacterial activities of inorganic agents on six bacteria associated with oral infections by two susceptibility tests. Int J Antimicrob Agents 27:513–517
64. Uhl L, Gerstel A, Chabalier M, Dukan S (2015) Hydrogen peroxide induced cell death: one or two modes of action. Heliyon 1:e00049
65. Chung I, Abdul Rahuman A, Marimuthu S, Vishnu Kirthi A, Anbarasan K, Padmini P, Rajakumar G (2017) Green synthesis of copper nanoparticles using *Eclipta prostrata* leaves extract and their antioxidant and cytotoxic activities. Exp Ther Med. https://doi.org/10.3892/etm.2017.4466
66. Ijaz F, Shahid S, Khan SA, Ahmad W, Zaman S (2017) Green synthesis of copper oxide nanoparticles using *Abutilon indicum* leaf extract: antimicrobial, antioxidant and photocatalytic dye degradation activities. Trop J Pharm Res 16:743
67. Rajeshkumar S, Rinitha G (2018) Nanostructural characterization of antimicrobial and antioxidant copper nanoparticles synthesized using novel *Persea americana* seeds. OpenNano 3:18–27
68. Rehana D, Mahendiran D, Kumar RS, Rahiman AK (2017) Evaluation of antioxidant and anticancer activity of copper oxide nanoparticles synthesized using medicinally important plant extracts. Biomed Pharmacother 89:1067–1077